Generalized framework for testing gravity with gravitational-wave propagation. II. Constraints on Horndeski theory

Shun Arai[1,*] and Atsushi Nishizawa[2]

[1]Department of Physics and Astrophysics, Nagoya University, Nagoya 464-8602, Japan
[2]Kobayashi-Maskawa Institute for the Origin of Particles and the Universe, Nagoya University, Nagoya 464-8602, Japan

(Received 17 November 2017; published 22 May 2018)

Gravitational waves (GW) are generally affected by modification of a gravity theory during propagation at cosmological distances. We numerically perform a quantitative analysis on Horndeski theory at the cosmological scale to constrain the Horndeski theory by GW observations in a model-independent way. We formulate a parametrization for a numerical simulation based on the Monte Carlo method and obtain the classification of the models that agrees with cosmic accelerating expansion within observational errors of the Hubble parameter. As a result, we find that a large group of the models in the Horndeski theory that mimic cosmic expansion of the ΛCDM model can be excluded from the simultaneous detection of a GW and its electromagnetic transient counterpart. Based on our result and the latest detection of GW170817 and GRB170817A, we conclude that the subclass of Horndeski theory including arbitrary functions G_4 and G_5 can hardly explain cosmic accelerating expansion without fine-tuning.

DOI: 10.1103/PhysRevD.97.104038

I. INTRODUCTION

As is already known, the expansion of the Universe is accelerating. From the first direct measurement of the cosmic accelerating expansion with type-Ia supernovae [1,2], subsequent observations of the cosmic microwave background (CMB) and surveys of large scale structure (LSS) have strongly suggested that the Λ cold dark matter (ΛCDM) model is the best explanation to describe the dynamical evolution of the late-time Universe [3,4]. However, the ΛCDM model is less supported from the theoretical point of view, because it has to assume the existence of unknown components that make up over 95% of the total in the Universe. Therefore, cosmic accelerating expansion remains one of the largest riddles of modern cosmology.

To solve this problem, two main ways have been proposed: dark energy and modified gravity. The former modifies only energy components of the Universe, leaving gravity to be described with general relativity (GR). For instance, quintessence [5] and the nonlinear kinetic term of a scalar field [6,7] are the models in the former category. The latter one, on the other hand, prescribes the cosmic accelerating expansion with a modification of gravity at the cosmological scale. Currently, in the case of modification with a scalar field, the universal description to treat dark energy and modified gravity together is called scalar-tensor theory. In particular, Horndeski theory [8,9] is the most general form of these theories, with a space-time curvature and a scalar field whose equations of motion contain up to second-order space-time derivatives. The Horndeski theory includes not only the quintessence and nonlinear kinetic theory, but also many specific theories: $f(R)$ theories [10], covariant Galileons [11,12], and kinetic gravity braiding [13]. The Horndeski theory can also be extended further to a more general framework in the language of an effective field theory (EFT). An EFT for dark energy was formulated by Gubitosi *et al.* [14], Gleyzes *et al.* [15,16], and Bellini and Sawicky [17].

With the EFT formulation, some alternative theories against the ΛCDM model have been examined using CMB and LSS observations [18]. However, one still needs to specify a model when calculating observables and comparing with observational data. This makes the analyses model dependent and may cause us to overlook the types of theories that are not classified into specific models. Therefore, it is important to investigate all of the subclasses in the Horndeski theory in a numerical way beyond analytical difficulties.

In the meantime, gravitational waves (GW) are gathering attention as a new tool to probe modified gravity. In fact, LIGO has succeeded at capturing GW for the first time [19]. LIGO has successively confirmed three more detections from the coalescence of binary black holes (BBH) [20–22] at cosmological distances. Moreover, the event rate of the detection of GW with the second-generation detector network at design sensitivity is expected to be 100–1000 yr^{-1}, which is statistically enough for cosmological applications.

*arai.shun@a.mbox.nagoya-u.ac.jp

As a result, we are able to extract cosmological information from the GW observations. For instance, GW are applicable to measure the Hubble constant [23–26].

For the application to constrain a modified gravity that explains the cosmic accelerating expansion, GW are a promising tool. In fact, Lombriser and Taylor [27] and Bettoni *et al.* [28] have reported that GW detections potentially distinguish the models of the Horndeski theory that describe the cosmic accelerating expansion. According to this paper, the detection of the phase velocity of GW, c_T, can exclude a wide range of the models that realize the accelerating expansion. This is because those models significantly displace c_T from the speed of light. It is known that the measurement of the deviation parameter δ_g, which is defined as $\delta_g \equiv 1 - c_T$, can reach down to $|\delta_g| \lesssim 10^{-15}$ with GW Cherenkov radiation [29] or electromagnetic counterparts for GW emission [30]. With these remarkable features, we expect GW to be a tool to search for the nature of the cosmic accelerating expansion.

In this paper, we develop the previous result in Lombriser and Taylor [27] to a numerical approach to test all possible Horndeski models and analyze the features imprinted on the propagation of GW. This paper is organized as follows. First of all, we review the previous study on the modification of the GW waveform during propagation in Sec. II. Next, in Sec. III we construct a model-independent method of parametrization to distinguish models in the Horndeski theory at cosmological scales. In Sec. IV, we compare with the analytical result in [27] a more qualitative way with Monte Carlo simulations. We find considerable deviation from their result. Finally, in Sec. V we obtain the distributions of models on the parameter plane, indicating that GW are the most efficient probe to constrain the models of modified gravity.

Very recently, LIGO and VIRGO detected a binary neutron star (BNS) merger named GW170817 [31]. This event is special because a few gamma-ray telescopes simultaneously caught the signal of a short gamma-ray burst, GRB170817A, and it was identified as the electromagnetic transient counterpart of GW170817. By using the difference of the arrival times between GW170817 and GRB170817A, they obtained a stringent constraint on δ_g down to $-7.0 \times 10^{-16} \lesssim \delta_g \lesssim 3.0 \times 10^{-15}$ [32]. Combining this result and our report, we conclude that the models in the Horndeski theory including the arbitrary functions G_4 and G_5 are not a main driver of the cosmic accelerating expansion. We will discuss this in Sec. V.

II. MODIFICATION OF GRAVITATIONAL-WAVE PROPAGATION AT COSMOLOGICAL SCALES

We briefly introduce how GW is deformed during propagation because of the modification of gravity. This argument was originally proposed by Saltas *et al.* [33] and recently it has been extended by Nishizawa to a general framework to test gravity theories [34]. In these papers, the propagation equation of GW is generally given by

$$h_{ij}'' + (2+\nu)\mathcal{H}h_{ij}' + (c_T^2 k^2 + a^2\mu^2)h_{ij} = a^2\Gamma\gamma_{ij}, \quad (1)$$

where h_{ij} is a tensor perturbation (GW) and $'$ denotes the derivative with respect to conformal time. In Eq. (1) there are four time-dependent parameters ν, c_T, μ, and Γ. ν is the Planck mass run rate, c_T is the phase velocity of a GW and μ is the graviton mass. Γ denotes extra sources generating GW. In the case that ν, c_T, μ are slowly varying functions with a cosmological timescale and there is no source, i.e., $\Gamma = 0$, the solution of Eq. (1) is given in [34] as

$$h = \mathcal{C}_{\rm MG} h_{\rm GR}, \quad (2)$$

where

$$\mathcal{C}_{\rm MG} \equiv e^{-\mathcal{D}} e^{-ik\Delta T}, \quad (3)$$

$$\mathcal{D} \equiv \frac{1}{2}\int^{\tau} d\tau' \nu\mathcal{H}, \quad (4)$$

$$\Delta T \equiv \int^{\tau} d\tau' \left\{\delta_g - \frac{a^2\mu^2}{2k^2}\right\}. \quad (5)$$

In Eq. (5) we replace $1 - c_T$ with the deviation parameter δ_g. $\mathcal{D}$ and ΔT correspond to the amplitude damping index and additional time delay of GW, respectively. We see that the damping parameter ν only appears in the GW amplitude, while δ_g and μ are both involved in the GW phase. In order to measure the arrival time difference between a GW and a photon, δ_g is small enough to make the time delay shorter than the timescale of GW observations. In Sec. V, we consider the case when δ_g is small.

III. NUMERICAL FORMULATION OF HORNDESKI THEORY AT COSMOLOGICAL SCALES

In this section we provide a numerical formulation of Horndeski theory independent of specific models. As we mentioned in Sec. I, the current observational analyses for the Horndeski theory are only limited to specific models. This is because the Horndeski theory is too general to investigate. Consequently, one can hardly extract information for which models are relatively favored from others under observational constraints. To tackle this difficulty, we perform a Monte Carlo simulation with a suitable parametrization independent of specific models. Although the number of parameters would become large, numerically this is not a problem. Now we construct a parametrization in the Horndeski theory in the following way. First of all,

we give a general Lagrangian density[1] of the Horndeski theory as

$$\mathcal{L} = \sum_{i=2}^{5} \mathcal{L}_i, \tag{6}$$

where

$$\mathcal{L}_2 = G_2(\phi, X), \tag{7}$$

$$\mathcal{L}_3 = -G_3(\phi, X)\Box\phi, \tag{8}$$

$$\mathcal{L}_4 = G_4(\phi, X)R + G_{4X}(\phi, X)[(\Box\phi)^2 - \phi_{;\mu\nu}\phi^{;\mu\nu}], \tag{9}$$

$$\mathcal{L}_5 = G_5(\phi, X)G_{\mu\nu}\phi^{;\mu\nu} - \frac{1}{6}G_{5X}(\phi, X)[(\Box\phi)^3 - 3\Box\phi_{;\mu\nu}\phi^{;\mu\nu} + 2\phi_{;\mu}{}^{;\nu}\phi_{;\nu}{}^{;\lambda}\phi_{;\lambda}{}^{;\mu}]. \tag{10}$$

Here $;_\mu$ is a covariant derivative and $X = -\phi_{;\mu}\phi^{;\mu}/2$, the canonical kinetic energy density of ϕ. The Lagrangian in Eq. (6) is the most general Lagrangian density in the Horndeski theory. What we now focus on is a phenomenon occurring at the Hubble timescale. In other words, we assume that gravity at small scales is irrelevant to our analysis at cosmological distances. This assumption is reasonable when testing GR at the cosmological scale due to nontrivial screening mechanisms in a nonlinear regime known as chameleon mechanisms [35] or Vainshtein mechanisms [36]. Indeed, Babichev *et al.* [37] and Kimura *et al.* [38] have successively reported that in the Horndeski theory the Vainshtein mechanism recovers GR at a short distance, while the time variation of gravitational coupling at cosmological distances remains unsuppressed. These facts indicate that we are justified in assuming that a GW waveform is modified only at the cosmological scale. As for a cosmological background, we define the flat Friedmann-Lemaître-Robertson-Walker (FLRW) metric as

$$ds^2 = -dt^2 + a^2(t)\delta_{ij}dx^i dx^j. \tag{11}$$

We now focus on the late time of the Universe below redshift $z = 1$. In this regime, time-dependent functions are approximately given by the Taylor expansion in powers of $H_0 t_{LB}$, where H_0 and t_{LB} are the Hubble constant and the look back time given by

$$t_{LB}(z) = \int_0^z \frac{dz'}{H(z')\cdot(1+z')}, \tag{12}$$

$$H(z) = H_0\sqrt{\Omega_{m0}(1+z)^3 + 1 - \Omega_{m0}}. \tag{13}$$

[1] $G_2(\phi, X)$ is often written $K(\phi, X)$ in literature.

Here $H(z)$ is the Hubble parameter and Ω_{m0} is the matter density parameter. As we will see in Sec. IV A we consider the two cases $\Omega_{m0} = 0.308$ (ΛCDM) and $\Omega_{m0} = 1$ [Einstein–de Sitter (EdS)] to give the Hubble parameter for each case. Now we expand the scalar field $\phi(t)$ as

$$\phi(t) \simeq M_\phi\left\{a_0 + a_1 H_0 t_{LB} + \frac{a_2}{2}(H_0 t_{LB})^2\right\}, \tag{14}$$

where M_ϕ is the mass scale of ϕ. Since M_ϕ normalizes ϕ, the coefficients $a_n (n = 0, 1, 2)$ can be chosen with the range $-1 < a_n < 1$.

Next we parametrize arbitrary functions $G_i (i = 2, 3, 4, 5)$ in the Horndeski theory as

$$G_i^{(\mathrm{app})}(\phi, X) \equiv \mathcal{G}_i\left\{g_i + \sum_{\rho=\hat{\phi},\hat{X}} g_{i\rho}\rho + \sum_{\rho,\sigma=\hat{\phi},\hat{X}} \frac{g_{i\rho\sigma}}{2}\rho\sigma + \sum_{\rho,\sigma,\lambda=\hat{\phi},\hat{X}} \frac{g_{i\rho\sigma\lambda}}{6}\rho\sigma\lambda\right\} \quad (i = 2, 3, 4, 5), \tag{15}$$

where $\hat{\phi}$ and $\hat{X}$ are dimensionless quantities given as $\mathrm{r}\hat{\phi} \equiv \phi/M_\phi$ and $\hat{X} \equiv \dot{\phi}^2/2H_0^2M_\phi^2$. Note that $|\hat{\phi}| < 1$ and $\hat{X} < 1$, which ensures the expansion given in Eq. (15). Throughout this paper, the dot is the derivative with respect to t, not t_{LB}. Note that $dt_{LB} = -dt$. g_i, $g_{i\rho}$, $g_{i\rho\sigma}$, and $g_{i\rho\sigma\lambda}$ in Eq. (15) are the model parameters set at random ranging from -1 to 1. $\mathcal{G}_i$ are normalization factors such as

$$\mathcal{G}_2 = M^4, \qquad \mathcal{G}_3 = \frac{M^4}{M_\phi H_0^2}, \qquad \mathcal{G}_4 = \frac{M^4}{H_0^2}, \qquad \mathcal{G}_5 = \frac{M^4}{M_\phi H_0^4}, \tag{16}$$

where $M \equiv \sqrt{M_{\mathrm{pl}}H_0}$ and M_{pl} is the reduced Planck mass. These normalization factors are determined in the way that the Lagrangian density of the system is of the order of $M_{\mathrm{pl}}^2 H_0^2 = M^4$.

The parametrization in Eqs. (14) and (15) is convenient for the numerical simulation we perform in Sec. IV. In the Horndeski theory, it takes too much time to collect all the models consistent with observations in the whole model space by solving the equations of motion. On the contrary, once $\phi(t)$ and $G_i(\phi, X)$ are given, it is able to avoid solving the equations of motion while we can check the validity of the given solutions numerically. To this end, a given form of $\phi(t)$ and $G_i(\phi, X)$ is useful to search the models that satisfy the observational conditions. This parametrization has in total 44 coefficients to distinguish models, which one is hardly able to obtain in analytical ways. Here is an advantage of the numerical approach with

the Monte Carlo method. Given $\phi(t)$ and $G_i(\phi, X)$, we can compute all variables, including α_M and α_T, which are relevant to GW observations. In the Horndeski theory, α_M and α_T are given by

$$M_*^2(t) \equiv 2(G_4 - 2XG_{4X} + XG_{5\phi} - \dot{\phi}HXG_{5X}), \quad (17)$$

$$\alpha_M(t) = \frac{1}{HM_*^2}\frac{dM_*^2}{dt}, \quad (18)$$

$$\alpha_T(t) = \frac{2X(2G_{4X} - 2G_{5\phi} - (\ddot{\phi} - \dot{\phi}H)G_{5X})}{M_*^2}. \quad (19)$$

α_M and α_T are related to the observable parameters ν and δ_g as

$$\nu = \alpha_M, \quad (20)$$

$$\delta_g = 1 - \sqrt{1 + \alpha_T}. \quad (21)$$

Note that $\delta_g \simeq -\alpha_T/2$ if δ_g is small. Substituting $\phi(t)$, the Hubble parameter in Eq. (12), and all $G_i^{(\mathrm{app})}$ in Eq. (15) into Eqs. (17)–(19), we can compute α_M and α_T as a function of redshift.

However, one has to be careful about the consistency of this formulation. According to our setup above, we give the Hubble parameter as in Eq. (13) while we assume the time dependence of $\phi(t)$ without solving the Friedmann equations of the system, which may cause inconsistency of the Hubble parameter. To avoid this, we have to impose an alternative criterion to obtain proper solutions. In the following section, we concretely implement our method with a Monte Carlo analysis by imposing additional criteria and show that this remedy appropriately finds the consistent models.

IV. MODEL CLASSIFICATION WITH MONTE CARLO SIMULATION

Next we classify models in the Horndeski theory into subgroups, depending on which arbitrary functions G_i play a role in accelerating the cosmic expansion. To this end, we now compute all physical quantities by randomly drawing all the coefficients from a uniform distribution, $[-1, 1]$, with a Monte Carlo method.

A. Consistency and stability conditions

As shown in Fig. 1, we filter the solutions by the following two conditions.

As shown in Fig. 1, two conditions are introduced: consistency and stability.

(i) Consistency:

Collecting the models whose cosmological time evolutions are H_{Horn} and $\dot{H}_{\mathrm{Horn}}$. H_{Horn} and $\dot{H}_{\mathrm{Horn}}$ are given by the Friedmann equations in Eqs. (A6) and (A7) in the Appendix. To obtain H_{Horn} and $\dot{H}_{\mathrm{Horn}}$, we substitute $H_{\Lambda\mathrm{CDM}}$ and $\phi(t)$ for the right-hand side of Eqs. (A8) and (A9). Then we impose the consistency criteria

$$|1 - H_{\mathrm{Horn}}/H_{\Lambda\mathrm{CDM}}| < 20\%, \quad (22)$$

$$|1 - \dot{H}_{\mathrm{Horn}}/\dot{H}_{\Lambda\mathrm{CDM}}| < 20\%. \quad (23)$$

Equations (22) and (23) work to select the models that pass the observational bound on the cosmic expansion by assessing the deviation from $H_{\Lambda\mathrm{CDM}}$ and $\dot{H}_{\Lambda\mathrm{CDM}}$. We choose the allowed range of estimation errors for the Hubble parameter up to 20% based on current variable observations of the Hubble parameter below $z = 0.1$, as shown in Table I of [39].

(ii) Stability:

Avoidance of ghost and gradient instabilities for the perturbations of scalar and tensor modes:

$$Q_s > 0, \quad c_s^2 > 0, \quad Q_T > 0, \quad c_T^2 > 0. \quad (24)$$

All of these quantities are given by Eqs. (A11)–(A13) in the Appendix, respectively. For the computation, we substitute $H = H_{\Lambda\mathrm{CDM}}$, $\dot{H} = \dot{H}_{\Lambda\mathrm{CDM}}$ in the quantities. Although we should use H_{Horn} to compute the quantities in Eq. (24), the difference of the quantities stays within observational errors. Hence the systematic misestimation of the stability condition associated with the choice of the Hubble parameter is negligibly small to sample consistent

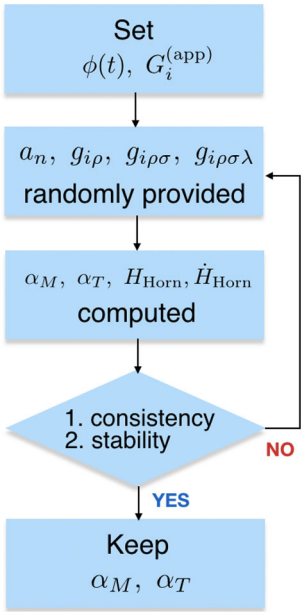

FIG. 1. The procedure to extract observationally reliable models with Monte Carlo simulation.

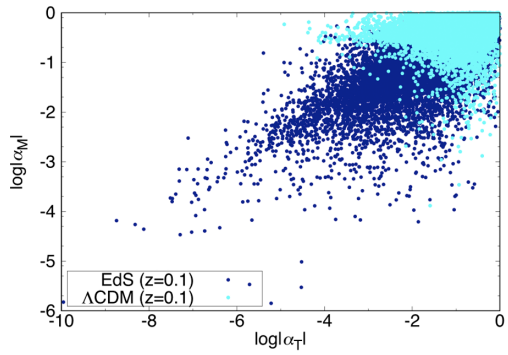

FIG. 2. Distribution of the models in the α_T-α_M plane with different cosmic expansion histories. The ΛCDM model (cyan dots) and the EdS model (dark blue dots) are considered.

models. Matter density $\tilde{\rho}_m$ and pressure $\tilde{p}_m$ are identified with cold dark matter density, such as $\tilde{\rho}_m = \Omega_{m0} a^{-3}/M_*^2$ and $\tilde{p}_m = 0$, respectively. The stability conditions guarantee linear perturbation at the cosmological scale.

In addition to the conditions above, we assume the following to make our discussion transparent. The third-order coefficients of G_2 or G_3 are set to be zero because these are not directly related to all the physical quantities considered above. Also, for simplicity, the current value of the scalar field ϕ_0 is set to zero, i.e., $a_0 = 0$, to recover GR at the present. To satisfy the condition $\phi_0 = 0$, we have to restrict the function G_2 in the form of $G_2 = g_2 + g_{2X}X + g_{2\phi\phi}\phi^2$.

B. Model distribution on the observables of gravitational waves

We show the distribution of models on the α_T-α_M plane, both of which are constrained from a GW measurement. In Sec. IV A, we explained the procedure to assign the values of all the parameters. Executing this procedure provides all the physical quantities, including α_T and α_M, at a referred redshift. We repeat the procedure and produce 1,000,000 discriminative models. In the following subsection, we firstly deal with a typical example, G_4, $G_5 \neq 0$, $G_2 = 0 = G_3$, and then we provide a general case in which all functions including G_2 and G_3 are switched on.

1. The effect of G_4 and G_5

The functions G_4 and G_5 play significant roles for α_T and α_M. In fact, one can see that α_T and α_M are determined solely by G_4 and G_5 in Eqs. (18) and (19). In addition, G_4 and G_5 can control the cosmic accelerating expansion. Because of their importance, we firstly perform our simulation while leaving G_4 and G_5 nontrivial and setting $G_2 = 0 = G_3$.

Firstly we see how the different histories of cosmic expansion affect the model distribution on the α_T-α_M plane. Here we refer to the cosmic expansion in the EdS universe. We now obtain the distribution in the case of the EdS just by replacing $H_{\Lambda\mathrm{CDM}}$ and $\dot{H}_{\Lambda\mathrm{CDM}}$ in Eqs. (22) and (23) with those of the EdS model, H_{EdS} and $\dot{H}_{\mathrm{EdS}}$, respectively. Figure 2 shows how distinctively the models distribute on the α_T-α_M plane under two different histories of the cosmic expansion. Moreover, to realize the cosmic expansion close to the case in the ΛCDM model with G_4 and G_5, either α_T or α_M must be $\mathcal{O}(1)$. This result is expected from the analytic estimation of Lombriser and Taylor [27], but the shape of our distribution is different in detail from theirs. The dots are very sparse at the top left or bottom right, where either α_T or α_M is extremely small. The main reason for this is due to the random sampling of models from all possible models. In other words, the models that have tiny values of α_M and α_T need fine-tuning to realize the cosmic expansion in the same way as the ΛCDM model.

2. Model classification on the α_T-α_M plane in general cases

We now allow all the model parameters to vary; namely, G_2 and G_3 are both nonzero. The parameters in Eqs. (14) and (15) are now provided at random. What we show in this section is how the models belonging to the different subclasses of the Horndeski theory are distributed on the α_T-α_M plane. For instance, quintessence and the scalar field with nonlinear kinetic theory are exactly at the point of $\alpha_T = 0 = \alpha_M$, while $f(R)$ theory is on the α_M axis ($\alpha_T = 0$). We now classify the models into four categories, as shown in Table I. Based on the classification, we carry out the Monte Carlo simulation and obtain the distributions of each subclass in Fig. 3.

As we see in Fig. 3, the models except the subclass (II) are distributed in the domain with large α_T. This is because in those cases G_4 and G_5 mainly drive the cosmic accelerating expansion and α_T consequently becomes large. In the subclass (II), on the contrary, the models diagonally concentrate toward the area in which both α_T and α_M are

TABLE I. Division of subclasses with parameters in $G_i^{(\mathrm{app})}$ and corresponding theories.

Subclass of Horndeski theory	Parameters of $G_i^{(\mathrm{app})}$	Models	References
(I) $G_4 + G_5$	G_2, $G_3 = 0$	Self-acceleration	[27]
(II) $G_4 + G_5 + G_2$	g_2, g_{2X}, $g_{2\phi\phi} \neq 0$	Quintessence/nonlinear kinetic theory/ $f(R)$ theories	[5,6,10,40]
(III) $G_4 + G_5 + G_3$	$G_3 \neq 0$	Cubic Galileons	[41,42]
(IV) Cov. Gal	$g_{2X}, g_{3X}, g_{4XX}, g_{5XX} \neq 0$	Covariant Galileons	[11,12]

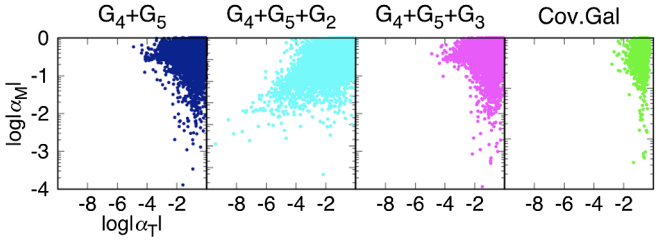

FIG. 3. Distribution of models in each subclass shown in Table I on the α_T-α_M plane.

small. This is because G_2 in turn plays a role in accelerating the cosmic expansion, which relaxes the constraints on G_4 and G_5. In this subclass, we also find that the models are predicted to align along the diagonal line, $|\alpha_T| \propto |\alpha_M|^2$. We discuss analytically why this feature appears in the following way. First of all, we assume that $\dot{\phi}$ is initially tiny and the time evolution of $\dot{\phi}$ is very slow as $|\ddot{\phi}/H\dot{\phi}| \ll 1$. In this case, we expand G_i as

$$G_i(\phi, X) \simeq G_i(\phi_0, X_0) - G_{i\phi}(\phi_0, X_0)\dot{\phi}_0 t_{LB}, \quad (25)$$

where the subscript 0 denotes the values at the present time. Hereafter we simplify the expressions $G_i(\phi_0, X_0) = G_{i,0}$ and $G_{i\rho}(\phi_0, X_0) = G_{i\rho,0}$, where $\rho = \phi$ or X. In the same way as in Eq. (25), we obtain the observable parameters α_M and α_T from Eqs. (17)–(19) as

$$\alpha_M \simeq \frac{G_{4\phi,0}}{G_{4,0}}\dot{\phi}_0, \quad (26)$$

$$\alpha_T \simeq \frac{2(G_{4\phi,0} - G_{5\phi,0})}{G_{4,0}} X_0. \quad (27)$$

Considering $X_0 = \dot{\phi}_0^2/2$, we obtain the relation between α_M and α_T as

$$\frac{\alpha_T}{\alpha_M^2} \simeq \frac{G_{4,0}(G_{4X,0} - G_{5\phi,0})}{{G_{4\phi,0}}^2} = \frac{g_4(g_{4X} - g_{5\phi})}{{g_{4\phi}}^2}. \quad (28)$$

Equation (28) is only valid if $g_{4\phi} = 0$. The second equality is obtained from Eq. (15). Since in our computation the model parameters are given by constants at random, we see that models are distributed along the line of $|\alpha_T| \propto |\alpha_M|^2$, which corresponds to a diagonal line on the α_T-α_M plane in the logarithmic scale.

Our analysis also suggests that the naive parametrization of α's is not always applicable. In the literature, it is widely accepted that the time evolution of all α's is proportional to the energy density of dark energy, $\alpha = \Omega_{\rm DE}\alpha_i$, where $\Omega_{\rm DE}(t) \equiv \tilde{\mathcal{E}}/3H_0^2$ and α_i is the initial value of α [17]. Indeed, this parametrization has proved to be valid in Galileon theories [43] and it is supported in cosmological surveys by Bayesian evidence [44]. However, as Linder has pointed out recently, this assumption is not always correct in the case of $f(R)$ gravity [45]. Our results also support this statement. Here we only see the correlation between α_T and α_M, but our technique is easily applicable to investigate the correlations among other parameters, including α_K and α_B. We will address this issue in a future publication.

V. OBSERVATIONAL CONSTRAINTS ON MODELS

As seen in the previous section, G_4 and G_5 induce the large deviation of α_T even in general cases. Next we derive the observational constraints on the Horndeski theory with GW propagation. Firstly we derive the analytic approximation for the observables of GW, which is applicable to the future observations of GW. Then we apply the expressions to the latest detection of GW170817 and GRB170817A to obtain the observational bound on the Horndeski theory.

From Eqs. (4), (5), (20), and (21), we can write down $\mathcal{D}$ and ΔT in terms of α_M and α_T. Note that $\mathcal{D}$ and ΔT are the observables given after integrating all effects between emission and detection. However, we are now interested in the case that all the quantities vary in the cosmological timescale. In such a case it is justified to use the Taylor expansion with respect to $H_0 t_{LB}$ as given in Eq. (14). As we introduced in Sec. II, ν and δ_g are the observational parameters that are model independent. With the definitions of the time evolution of ν and δ_g as

$$\nu = \nu_0 - \nu_1 H_0 t_{LB}, \quad (29)$$

$$\delta_g = \delta_{g0} - \delta_{g1} H_0 t_{LB}, \quad (30)$$

expanding up to the next-to-leading order in $H_0 t_{LB}$ gives the approximated expressions of Eqs. (4) and (5) as

$$\mathcal{D} \simeq \frac{1}{2}\left\{\nu_0 \ln(1+z) - \frac{\nu_1}{2}(H_0 t_{LB})^2\right\}, \quad (31)$$

$$\Delta T \simeq \frac{1}{H_0}\left\{\delta_{g0} H_0 t_{LB} - \frac{\delta_{g1}}{2}(H_0 t_{LB})^2\right\}. \quad (32)$$

Since we consider the Horndeski theory, ν and δ_g are given as a function of α_M and α_T. Expanding both sides of Eqs. (20) and (21) with respect to $H_0 t_{LB}$ and assuming δ_g to be considerably small, we obtain ν_0, ν_1, δ_{g0}, and δ_{g1} as

$$\nu_0 = \alpha_{M,0}, \quad (33)$$

$$\nu_1 = \frac{\dot{\alpha}_{M,0}}{H_0}, \quad (34)$$

$$\delta_{g0} = -\frac{\alpha_{T,0}}{2}, \quad (35)$$

$$\delta_{g1} = -\frac{\dot{\alpha}_{T,0}}{2H_0}. \quad (36)$$

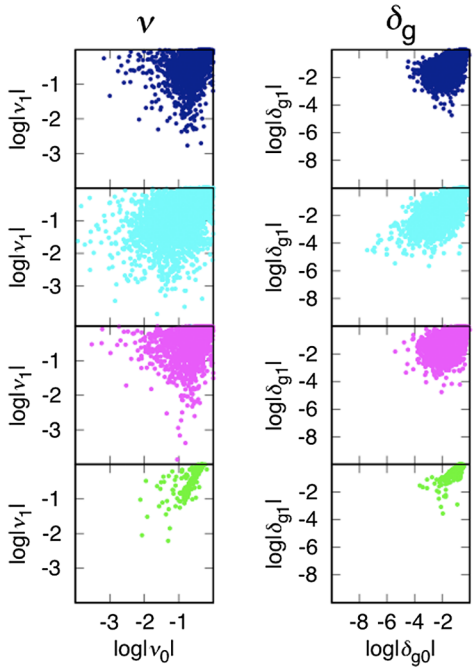

FIG. 4. Model distributions on the observable parameter plane for the subclasses shown in Table I. Each color of the dots corresponds to that in Fig. 3.

Converting the model parameters in the previous section to those in Eqs. (33)–(36), we obtain the distributions of the observable parameters as shown in Fig. 4. Similar to Figs. 4 and 5 shows that the effect of the G_4 and G_5 functions is distinguishable in both parameters ν and δ_g, while Fig. 4 additionally shows the information about the time evolution of the models in terms of ν_1 and δ_{g1}.

We now give observational constraints on ν_0, ν_1, δ_{g0}, and δ_{g1} from the detection of GW170817 and GRB170817A. The reason to choose this GW event is that the redshift of the GW is independently measured from the optical follow-up observation of NGC4993 [46], which resolves the degeneracy between the redshift and the luminosity distance in the GW observation. For the observables, $\mathcal{D}$ and ΔT, we have to take into account their estimation errors. In the case of measuring the arrival time difference, errors arise due to the accuracy of time resolution and intrinsic time delay at the source. As mentioned in the paper [30], the time resolution is sufficient so that we ignore the timing error and consider only the arrival time difference. As we see in [31], the arrival time difference is measured as 1.7 s, which gives the upper bound on c_T. We also set the intrinsic time delay at the source to 10 s to obtain the lower bound of c_T.

The constraint on ν is given by comparison between the observed luminosity distance and the computed one using redshift determined by optical observations. As shown in [31], the observed luminosity distance is given with error as 40^{+8}_{-14} Mpc. The computed luminosity distance at a given redshift is obtained once we assume the cosmology.

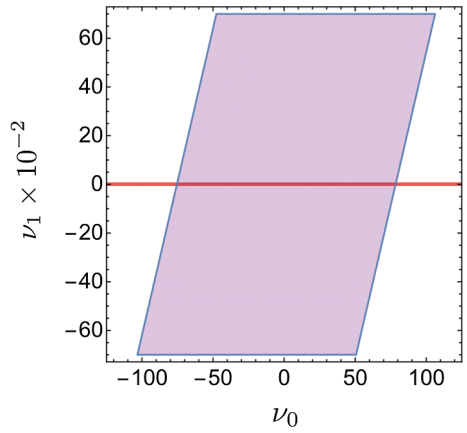

FIG. 5. Observational constraint on ν_0 and ν_1. The width of the colored region is given at a 1σ confidence level of the GW observation. The red solid line is $\nu_1 = 0$.

To obtain the computed luminosity distance, H_0, and t_{LB}, we take the cosmology to the best fit ΛCDM model in [4], i.e., $H_0 = 67.8\ \mathrm{km\,s^{-1}\,Mpc^{-1}}$ and $\Omega_{m0} = 0.308$ as prior values to maintain consistency with the CMB observation. We are interested in the models that explain the cosmic accelerating expansion at low redshifts $z < 1$ while recovering the standard ΛCDM cosmology at higher redshifts $z > 1$. To keep the consistency of the models, we set H_0 and Ω_{m0} to fit with the CMB observation.

After all the procedures, we finally obtain the constraints as shown in Figs. 5 and 6. Comparing the left panel in Fig. 4 with Fig. 5, we find that ν_0 and ν_1 are loosely constrained, but not enough to distinguish the models in Table I. By contrast, in the right panel of Fig. 4 and in Fig. 6, all the models are excluded by the single observation of GW170817 unless one carries out exceptional fine-tuning for the models. Consequently, we conclude that the

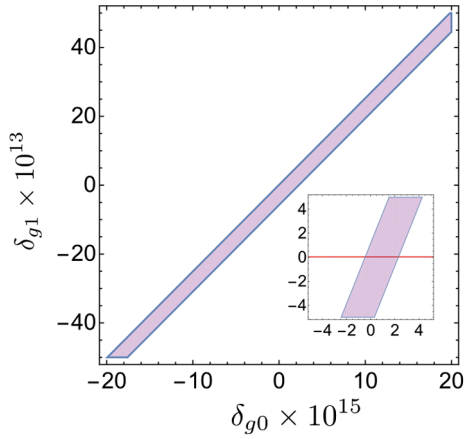

FIG. 6. Observational constraint on δ_0 and δ_1. The width of the colored region is given between the lower and upper bounds. Inset: The enlarged version around the center of the figure. The width of the colored region is given at a 1σ confidence level of the GW observation. The red solid line is $\delta_{g1} = 0$.

models in the Horndeski theory that include G_4 or G_5 without G_2 can be excluded unless the model parameters are fine-tuned so that $c_T = 1$. The models in subclass (II) are such that quintessence, nonlinear kinetic theory, or $f(R)$ theories survive because these models satisfy $c_T = 1$. In other words, without fine-tuning for the G_4 and G_5 functions, the cosmic expansion must be driven by the G_2 function.

If we take the cases that $\nu_1 = 0$ or $\delta_{g1} = 0$, we obtain the constraints on ν_0 and δ_{g0} as

$$-75.3 \leq \nu_0 \leq 78.4, \tag{37}$$

$$-4.7 \times 10^{-16} \leq \delta_{g0} \leq 2.2 \times 10^{-15}. \tag{38}$$

ν_0 is too loose to constrain the models in Table I, while δ_{g0} is well determined enough to exclude the models. The constraint of δ_{g0} is consistent with the one in [32].

Finally, we comment on a future prospect of tightening the constraints. In the above, we used a single source to constrain the Horndeski theory. However, given multiple sources at different distances in the future observation, one can tighten the constraint by combining the sources in two ways [47]. First with a single source, there exists a parameter degeneracy in the time evolution, as shown by the shaded bands in Figs. 5 and 6. If one uses multiple sources at different distances, the bands cross at a point and the degeneracy is broken. Second, currently the intrinsic time delay limits the sensitivity to δ_g. However, the intrinsic time delay can be distinguished from the modification of GW propagation and partially canceled out by combining multiple signals. This is possible because those effects depend on redshift differently at cosmological distances.

VI. CONCLUSIONS

In this paper, we have discussed constraints on Horndeski theory with GW propagation. We firstly reviewed the general framework for the waveform deformation from modified gravity, including the Horndeski theory. Then we numerically formulated the Horndeski theory at the cosmological scale to compute α_M and α_T.

Next, we performed a Monte Carlo simulation that keeps the models consistent with the observations of cosmic expansion. In this procedure, we adopted two criteria: consistency and stability. Carrying out the simulation, we obtained the model distribution on the α_T-α_M plane. Then we found that α_M and α_T have large values in the models including only G_4 or G_5, while including G_2 together with G_4 or G_5 allows both α_M and α_T to be smaller. Thanks to this feature, the models are significantly distinguishable depending on whether or not the models include the function G_2.

Finally, we constrained the Horndeski theory from the simultaneous detection of GW170817 and GRB170817A. We provided the observational bounds for the physical parameters that are involved in GW propagation: $\nu_0, \nu_1, \delta_{g0}$, and δ_{g1}. As a result, we found that the constraints on ν_0 and ν_1 are still too weak to distinguish the specific models shown in the Table I, while those on δ_{g0} and δ_{g1} are sufficiently strong enough to exclude the models that contain G_4 or G_5 without G_2. Consequently, we concluded that the model space of the Horndeski theory must be significantly reduced to explain the cosmic accelerating expansion and the GW propagation simultaneously. In other words, in the Horndeski framework the main driver of the cosmic accelerating expansion should be G_2. At present, the models such as quintessence, nonlinear kinetic theory, or $f(R)$ theories are still allowed.

In addition to our work, we comment on the theories other than the Horndeski theory, including higher derivatives of a scalar curvature and a scalar field. Our formulation in effect contains those theories because the higher derivative terms become too tiny to be observed at the cosmological scale. This argument agrees with the recent reports just after the detection of GW170817 was announced [48–51]. However, our work quantitatively discusses how much the fine-tuning of the model is required within the current observational errors. In addition, as shown in Eq. (37), we obtained for the first time the constraint on the amplitude damping parameter ν by the observation of GW170817. Although the constraint is loose, it plays an important role in further restricting the models whose δ_g is fine-tuned to zero.

In the end, we report on an accidental finding that the parametrization of $\alpha \propto \Omega_{\rm DE}\alpha_i$ is not valid in general. This assumption is now widely used when computing cosmological observables, particularly the CMB angular power spectrum, using Einstein-Boltzmann solvers [52–54]. Therefore, it is important to revisit the previous constraints on the Horndeski theory that parametrized $\alpha \propto \Omega_{\rm DE}\alpha_i$ and to investigate the application of our simulation to other cosmological observations such as CMB or LSS. We will address this issue in a future publication.

ACKNOWLEDGMENTS

S. A. is supported by a Grant-in-Aid for the Japan Society for the Promotion of Science Research under Grant No. 17J04978. This work was supported by JSPS KAKENHI Grant No. JP17H06358.

APPENDIX: COMPUTATION OF MODEL PARAMETERS

We introduce physical quantities necessary for computation in the main text. Here we use the α parametrization of Bellini and Sawacki [17]. First of all, the time-evolving the parameters are defined as

$$M_*^2 \equiv 2(G_4 - 2XG_{4X} + XG_{5\phi} - \dot{\phi}HXG_{5X}), \tag{A1}$$

$$HM_*^2\alpha_M \equiv \frac{d}{dt}M_*^2, \tag{A2}$$

$$\begin{aligned} H^2M_*^2\alpha_K \equiv & 2X(G_{2X}+2XG_{2XX}-2G_{3\phi}-2XG_{3\phi X}) \\ & +12\dot{\phi}XH(G_{3X}+XG_{3XX}-3G_{4\phi X}-2XG_{4\phi XX}) \\ & +12XH^2(G_{4X}+8XG_{4XX}+4X^2G_{4XXX}) \\ & -12XH^2(G_{5\phi}+5XG_{5\phi X}+2X^2G_{5XXX}) \\ & +4\dot{\phi}XH^3(3G_{5X}+7XG_{5XX}+2X^2G_{5XXX}), \end{aligned} \tag{A3}$$

$$\begin{aligned} HM_*^2\alpha_B \equiv & 2\dot{\phi}(XG_{3X}-G_{4\phi}-2XG_{4\phi X}) \\ & +8XH(G_{4X}+2XG_{4XX}-G_{5\phi}-XG_{5\phi X}) \\ & +2\dot{\phi}XH^2(3G_{5X}+2XG_{5XX}), \end{aligned} \tag{A4}$$

$$M_*^2\alpha_T \equiv 2X(2G_{4X}-2G_{5\phi}-(\ddot{\phi}-\dot{\phi}H)G_{5X}). \tag{A5}$$

Of all the four parameters, α_M and α_T are relevant to GW propagation. α_K and α_B are irrelevant to GW propagation, but they are necessary to evaluate the stability condition discussed in Sec. IV A. The Friedman equations in the Horndeski theory are given by

$$3H^2 = \tilde{\rho}_m + \tilde{\mathcal{E}}, \tag{A6}$$

$$2\dot{H} + 3H^2 = -\tilde{p}_m - \tilde{\mathcal{P}}, \tag{A7}$$

where $\tilde{\rho}_m \equiv \rho_m/M_*^2$ and $\tilde{p}_m \equiv p_m/M_*^2$. Then $\tilde{\mathcal{E}}$ and $\tilde{\mathcal{P}}$ are given by

$$\begin{aligned} M_*^2\tilde{\mathcal{E}} = & -G_2 + 2X(G_{2X}-G_{3\phi}) \\ & +6\dot{\phi}H(XG_{3X}-G_{4\phi}-2XG_{4\phi X}) \\ & +12H^2X(G_{4X}+2XG_{4XX}-G_{5\phi}-XG_{5\phi X}) \\ & +4\dot{\phi}H^3X(G_{5X}+XG_{5XX}), \end{aligned} \tag{A8}$$

$$\begin{aligned} M_*^2\tilde{\mathcal{P}} = & G_2 - 2X(G_{3\phi}-2G_{4\phi\phi}) \\ & +4\dot{\phi}H(G_{4\phi}-2XG_{4\phi X}+XG_{5\phi\phi}) \\ & -M_*^2\alpha_BH\frac{\ddot{\phi}}{\dot{\phi}} - 4H^2X^2G_{5\phi X} + 2\dot{\phi}H^3XG_{5X}. \end{aligned} \tag{A9}$$

As we can see in all the quantities above, the third derivatives of G_2 and G_3 implicitly affect the quantities. Therefore, we set the third derivatives of G_2 and G_3 to be zero in the main text.

Finally, we provide essential quantities to avoid the ghost and gradient instability. The action at quadratic order of a scalar field ζ and tensor modes h_{ij} is given by

$$\begin{aligned} S_2 = \int dtd^3xa^3\Bigg[& Q_s\left(\dot{\zeta}^2 - \frac{c_s^2}{a^2}(\partial_i\zeta)^2\right) \\ & + Q_T\left(\dot{h}_{ij}^2 - \frac{c_T^2}{a^2}(\partial_k h_{ij})^2\right)\Bigg], \end{aligned} \tag{A10}$$

where

$$\begin{aligned} Q_s &= \frac{2M_*^2D}{(2-\alpha_B)^2}, \\ c_s^2 &= -\frac{(2-\alpha_B)}{H^2D}\Bigg[\dot{H} - \frac{1}{2}H^2\alpha_B(1+\alpha_T) \\ & \quad - H^2(\alpha_M-\alpha_T) - H\dot{\alpha}_B + \tilde{\rho}_m + \tilde{p}_m\Bigg], \end{aligned} \tag{A11}$$

$$D \equiv \alpha_K + \frac{3}{2}\alpha_B^2, \tag{A12}$$

while

$$Q_T = \frac{M_*^2}{8}, \tag{A13}$$

$$c_T^2 = 1 + \alpha_T. \tag{A14}$$

To avoid the theoretical instabilities, we should impose the condition that $Q_s > 0$, $c_s^2 > 0$, $Q_T > 0$, and $c_T^2 > 0$.

[1] A. G. Riess *et al.*, Observational evidence from supernovae for an accelerating universe and a cosmological constant, Astron. J. **116**, 1009 (1998).

[2] S. Perlmutter *et al.*, Measurements of Ω and Λ from 42 high redshift supernovae, Astrophys. J. **517**, 565 (1999).

[3] E. Komatsu *et al.*, Seven-year Wilkinson Microwave Anisotropy Probe (WMAP) observations: Cosmological interpretation, Astrophys. J. Suppl. Ser. **192**, 18 (2011).

[4] P. A. R. Ade *et al.* (Planck Collaboration), Planck 2015 results. XIII. Cosmological parameters, Astron. Astrophys. **594**, 63 (2015).

[5] J. P. E. Peebles and B. Ratra, The cosmological constant and dark energy, Rev. Mod. Phys. **75**, 559 (2003).

[6] T. Chiba, T. Okabe, and M. Yamaguchi, Kinetically driven quintessence, Phys. Rev. D **62**, 023511 (2000).

[7] C. Armendariz-Picon, V. Mukhanov, and P. J. Steinhardt, Essentials of k-essence, Phys. Rev. D **63**, 103510 (2001).
[8] G. W. Horndeski, Second-order scalar-tensor field equations in a four-dimensional space, Int. J. Theor. Phys. **10**, 363 (1974).
[9] T. Kobayashi, M. Yamaguchi, and J. Yokoyama, Generalized G-inflation: Inflation with the most general second-order field equations, Prog. Theor. Phys. **126**, 511 (2011).
[10] A. De Felice and S. Tsujikawa, f(R) theories, Living Rev. Relativ. **13**, 3 (2010).
[11] C. Deffayet, G. Esposito-Farése, and A. Vikman, Covariant Galileon, Phys. Rev. D **79**, 084003 (2009).
[12] A. Nicolis, R. Rattazzi, and E. Trincherini, The galileon as a local modification of gravity, Phys. Rev. D **79**, 064036 (2009).
[13] C. Deffayet, O. Pujolas, I. Sawicki, and A. Vikman, Imperfect dark energy from kinetic gravity braiding, J. Cosmol. Astropart. Phys. 10 (**2010**) 026.
[14] G. Gubitosi, F. Piazza, and F. Vernizzi, The effective field theory of dark energy, J. Cosmol. Astropart. Phys. 02 (2013) 032.
[15] J. Gleyzes, D. Langois, F. Piazza, and F. Vernizzi, Essential building blocks of dark energy, J. Cosmol. Astropart. Phys. 08 (2013) 025.
[16] J. Gleyzes, D. Langois, M. Mancarella, and F. Vernizzi, Effective theory of interacting dark energy, J. Cosmol. Astropart. Phys. 08 (2015) 054.
[17] E. Bellini and I. Sawicki, Maximal freedom at minimum cost: Linear large scale structure in general modification of gravity, J. Cosmol. Astropart. Phys. 07 (2014) 050.
[18] E. Bellini, A. J. Cuesta, R. Jimenez, and L. Verde, Constraints on deviations from ΛCDM within Horndeski gravity, Astron. Astrophys. **584**, A35 (2015).
[19] B. P. Abbott *et al.* (LIGO Scientific and Virgo Collaborations), Observation of Gravitational Waves from a Binary Black Hole Merger, Phys. Rev. Lett. **116**, 061102 (2016).
[20] B. P. Abbott *et al.* (LIGO Scientific and Virgo Collaborations), GW151226: Observation of Gravitational Waves from a 22-Solar-Mass Binary Black Hole Coalescence, Phys. Rev. Lett. **116**, 241103 (2016).
[21] B. P. Abbott *et al.* (LIGO Scientific and Virgo Collaborations), GW170104: Observation of a 50-Solar-Mass Binary Black Hole Coalescence at Redshift 0.2, Phys. Rev. Lett. **118**, 221101 (2017).
[22] B. P. Abbott *et al.* (LIGO Scientific and Virgo Collaborations), GW170814: A Three-Detector Observation of Gravitational Waves from a Binary Black Hole Coalescence, Phys. Rev. Lett. **119**, 141101 (2017).
[23] B. F. Schutz, Determining the Hubble constant from gravitational wave observations, Nature (London) **323**, 310 (1986).
[24] S. Nissanke, D. E. Holz, N. Dalal, S. A. Hughes, J. L. Sievers, and C. M. Hirata, Determining the Hubble constant from gravitational wave observations of merging compact binaries, arXiv:1307.2638.
[25] A. Nishizawa, Measurement of Hubble constant with stellar-mass binary black holes, Phys. Rev. D **96**, 101303 (2017).
[26] LIGO Scientific Collaboration, Virgo Collaboration, 1M2H Collaboration, Dark Energy Camera GW-EM Collaboration, DES Collaboration, DLT40 Collaboration, Las Cumbres Observatory Collaboration, VINROUGE Collaboration, and MASTER Collaboration, A gravitational-wave standard siren measurement of the Hubble constant, Nature (London) **551**, 85 (2017).
[27] L. Lombriser and A. Taylor, Breaking a dark degeneracy with gravitational waves, J. Cosmol. Astropart. Phys. 03 (2016) 031.
[28] D. Bettoni, J. M. Ezquiaga, K. Hinterbichler, and M. Zumalacárregui, Breaking a dark degeneracy with gravitational waves, Phys. Rev. D **95**, 084029 (2017).
[29] G. D. Moore and A. E. Nelson, Lower bound on the propagation speed of gravity from gravitational Cherenkov radiation, J. High Energy Phys. 023 (2001) 0109.
[30] A. Nishizawa and T. Nakamura, Measuring speed of gravitational waves by observations of photons and neutrinos from compact binary mergers and supernovae, Phys. Rev. D **90**, 044048 (2014).
[31] B. P. Abbott (LIGO Scientific Collaboration and Virgo Collaboration), GW170817: Observation of Gravitational Waves from a Binary Neutron Star Inspiral, Phys. Rev. Lett. **119**, 161101 (2017).
[32] B. P. Abott *et al.*, Gravitational waves and gamma-rays from a binary neutron star merger: GW170817 and GRB 170817A, Astrophys. J. Lett. **848**, L13 (2017).
[33] I. Saltas, I. Sawicki, L. Amendola, and M. Kunz, Anisotropic Stress as Signature of Non-standard Propagation of Gravitational Waves, Phys. Rev. Lett. **113**, 191101 (2014).
[34] A. Nishizawa, preceding article, Generalized framework for testing gravity with gravitational-wave propagation. I. Formulation, Phys. Rev. D **97**, 104037 (2018).
[35] J. Khoury and A. Weltman, Chameleon cosmology, Phys. Rev. D **69**, 044026 (2004).
[36] A. I. Vainstein, To the problem of nonvanishing gravitation mass, Phys. Lett. **39B**, 393 (1972).
[37] E. Babichev, C. Deffayet, and G. Esposito-Farése, Constraints on Shift-Symmetric Scalar-Tensor Theories with a Vainshtein Mechanism from Bounds on the Time Variation of G, Phys. Rev. Lett. **107**, 251102 (2011).
[38] R. Kimura, T. Kobayashi, and Y. Yamamoto, Vainshtein screening in a cosmological background in the most general second-order scalar-tensor theory, Phys. Rev. D **85**, 024023 (2012).
[39] O. Farooq, F. R. Madiyar, S. Crandall, and B. Ratra, Hubble parameter measurement constraints on the redshift of the deceleration-acceleration transition, dynamical dark energy, and space curvature, Astrophys. J. **835**, 26 (2017).
[40] Y. S. Song, W. Hu, and I. Sawicki, The large scale structure of $f(R)$ gravity, Phys. Rev. D **75**, 044004 (2007).
[41] E. Bellini and R. Jimenez, The parameter space of cubic Galileon models for cosmic acceleration, Phys. Dark Universe **2**, 179 (2013).
[42] A. Barreira, B. Li, W. A. Hellwing, C. M. Baugh, and S. Pascoli, Nonlinear structure formation in the cubic Galileon gravity model, J. Cosmol. Astropart. Phys. 10 (2013) 027.
[43] J. Renk, M. Zumalacarregui, and F. Montanari, Gravity at the horizon: On relativistic effects, CMB-LSS correlations and ultra-large scales in Horndeski's theory, J. Cosmol. Astropart. Phys. 07 (2016) 040.

[44] J. Gleyzes, Parametrizing modified gravity for cosmological surveys, Phys. Rev. D **96**, 063516 (2017).
[45] E. Linder, Challenges in connecting modified gravity theory and observations, Phys. Rev. D **95**, 023518 (2017).
[46] LIGO Scientific Collaboration, Virgo Collaboration, Fermi GBM, INTEGRAL, IceCube Collaboration, AstroSat Cadmium Zinc Telluride Imager Team, IPN Collaboration, Insight-Hxmt Collaboration, ANTARES Collaboration, Swift Collaboration, AGILE Team, 1M2H Team, Dark Energy Camera GW-EM Collaboration, DES Collaboration, DLT40 Collaboration, GRAWITA: GRAvitational Wave Inaf TeAm, Fermi Large Area Telescope Collaboration, ATCA: Australia Telescope Compact Array, ASKAP: Australian SKA Pathfinder, Las Cumbres Observatory Group, OzGrav, DWF (Deeper, Wider, Faster Program), AST3 and CAASTRO Collaborations, VINROUGE Collaboration, MASTER Collaboration, J-GEM, GROWTH, JAGWAR, CaltechNRAO, TTU-NRAO, and NuSTAR Collaborations, Pan-STARRS, MAXI Team, TZAC Consortium, KU Collaboration, Nordic Optical Telescope, ePESSTO, GROND, Texas Tech University, SALT Group, TOROS: Transient Robotic Observatory of the South Collaboration, BOOTES Collaboration, MWA: Murchison Widefield Array, CALET Collaboration, IKI-GW Follow-up Collaboration, H.E.S.S. Collaboration, LOFAR Collaboration, LWA: Long Wavelength Array, HAWC Collaboration, Pierre Auger Collaboration, ALMA Collaboration, Euro VLBI Team, Pi of the Sky Collaboration, The Chandra Team at McGill University, DFN: Desert Fireball Network, ATLAS, High Time Resolution Universe Survey, RIMAS and RATIR, and SKA South Africa/MeerKAT, Multi-messenger observations of a binary neutron star merger, Astrophys. J. Lett. **848**, L12 (2017).
[47] A. Nishizawa, Constraining the propagation speed of gravitational waves with compact binaries at cosmological distances, Phys. Rev. D **93**, 124036 (2016).
[48] P. Creminelli and F. Vernizzi, Dark Energy after GW170817, Phys. Rev. Lett. **119**, 251302 (2017).
[49] J. Sakstein and B. Jain, Implications of the Neutron Star Merger GW170817 for Cosmological Scalar-Tensor Theories, Phys. Rev. Lett. **119**, 251303 (2017).
[50] J. M. Ezquiaga and M. Zumalacárregui, Dark Energy after GW170817, Phys. Rev. Lett. **119**, 251304 (2017).
[51] J. M. Ezquiaga and M. Zumalacárregui, Dark Energy after GW170817: Dead Ends and the Road Ahead, Phys. Rev. Lett. **119**, 251304 (2017).
[52] B. Hu, M. Raveri, N. Frusciante, and A. Silvestri, Effective field theory of cosmic acceleration: An implementation in CAMB, Phys. Rev. D **89**, 103530 (2014).
[53] M. Zumalacarregui, E. Bellini, I. Sawicki, J. Lesgourgues, and P. G. Ferreira, hi_class: Horndeski in the cosmic linear anisotropy solving system, J. Cosmol. Astropart. Phys. 08 (2017) 019.
[54] E. Bellini *et al.*, A comparison of Einstein-Boltzmann solvers for testing general relativity, Phys. Rev. D **97**, 023520 (2018).